ADVANCED ELECTRONIC MATERIALS
www.advelectronicmat.de

Tunable Electronic Structures in Wrinkled 2D Transition-Metal-Trichalcogenide (TMT) $HfTe_3$ Films

Yu-Qi Wang, Xu Wu, Yan-Feng Ge, Ye-Liang Wang, Haiming Guo, Yan Shao, Tao Lei, Chen Liu, Jia-Ou Wang, Shi-Yu Zhu, Zhong-Liu Liu, Wei Guo, Kurash Ibrahim, Yu-Gui Yao, and Hong-Jun Gao**

2D materials with anisotropic symmetry are likely, in general, to possess strain that is artificially adjustable in a single direction, inspiring strategies of artificial regulation of local structures and related properties. Herein, strain-induced wrinkles in an anisotropic 2D transition-metal-trichalcogenide $HfTe_3$ film are fabricated and illustrated for the first time. The corresponding localized electronic structures in the 1D corrugated wrinkles are revealed by a combination of experiment and simulation. The wrinkled $HfTe_3$ film probably features electrical transport properties never before seen and useful for developing wrinkle-based heterojunctions for novel nanoelectronic devices.

1. Introduction

In layered 2D materials, strain normally exists due to differences in both atomic thickness and symmetry among adjacent layers. Recent studies of 2D materials demonstrate that strain can affect their local structures and hence induce many properties not previously observed.[1–13] These materials include graphene,[1–6,14] hexagonal boron nitride (hBN),[15,16] transition-metal dichalcogenides (TMD),[10–12,17,18] and so on. These 2D materials are isotropically symmetric with a hexagonal lattice. Besides these 2D material systems, layered transition-metal-trichalcogenide (TMT), on one hand, also has a 2D sandwiched configuration similar to TMD. TMT has the general formula MX_3 (M = transition metal and X = chalcogenide). Monolayer MX_3 has a layered configuration, with a sublayer of M combined by two sublayers of X elements. On the other hand, TMT has anisotropic rectangular symmetry, unlike the isotropic hexagonal symmetry in TMD. The anisotropic symmetry of TMT allows easy formation of strain-induced structures in a particular direction and thus unheard-of properties in such materials for potential application in sensors or nanoelectronic devices. However, reports on strain-induced structures and properties are still rare on this kind of anisotropic 2D material systems.

Specifically, a single-layer $HfTe_3$ film consists of trigonal prismatic chains that are arranged in parallel with Hf—Te bonds (see schematic in **Figure 1**).[19,20] It has an anisotropic rectangular symmetry. Because the Hf—Te bonds connecting the trigonal prismatic chains are longer than the Hf—Te bonds in the trigonal prismatic chains, stretching or compressing $HfTe_3$ films along the direction parallel to the trigonal prismatic chains is easier than along the direction perpendicular to the trigonal prismatic chains. So $HfTe_3$ films can be stretched or compressed in a certain direction and might be used in electronic devices modulated by surface strain.

Here, we report on strain-induced wrinkles in the anisotropic $HfTe_3$ film and the material's local electronic properties, investigated by scanning tunneling microscopy/spectroscopy (STM/STS), X-ray photoelectron spectroscopy (XPS) measurements, and density functional theory (DFT) calculations. Figure 1a–c shows schematics of a flat $HfTe_3$ film on Hf(0001) substrate. We can see the difference in symmetry between the $HfTe_3$ film and Hf(0001) substrate. The $HfTe_3$ film has a rectangular symmetry and the Hf(0001) substrate has a hexagonal symmetry (Figure 1b,c). The surface lattice constants of Hf(0001) substrate are 3.20 Å in the *a*-direction and 5.54 Å in the *c*-direction, respectively. The lattice periodicities of $HfTe_3$ bulk are 3.90 Å in the *a*-direction and 5.90 Å in the *c*-direction, respectively.[19] The lattice mismatch is ≈6.5% in *c*-direction and ≈20% in the *a*-direction. The obvious mismatch of lattice constant periods

Y.-Q. Wang, X. Wu, Prof. Y.-L. Wang, Dr. H. Guo, Y. Shao, S.-Y. Zhu, Z.-L. Liu, Prof. H.-J. Gao
Institute of Physics
Chinese Academy of Sciences
Beijing 100190, China
E-mail: ylwang@iphy.ac.cn; hjgao@iphy.ac.cn
Y.-Q. Wang, X. Wu, Prof. Y.-L. Wang, Dr. H. Guo, Y. Shao, S.-Y. Zhu, Z.-L. Liu, Prof. H.-J. Gao
Beijing Key Laboratory for Nanomaterials and Nanodevices
Beijing 100190, China
Y.-F. Ge, Dr. W. Guo, Prof. Y.-G. Yao
School of Physics
Beijing Institute of Technology
Beijing 100081, China
Prof. Y.-L. Wang, Prof. H.-J. Gao
School of Physics
University of Chinese Academy of Sciences
Beijing 100190, China
Prof. Y.-L. Wang, Prof. H.-J. Gao
Collaborative Innovation Center of Quantum Matter
Beijing 100084, China
T. Lei, C. Liu, Dr. J.-O. Wang, Prof. K. Ibrahim
Institute of High Energy Physics
Chinese Academy of Sciences
Beijing 100049, China

DOI: 10.1002/aelm.201600324

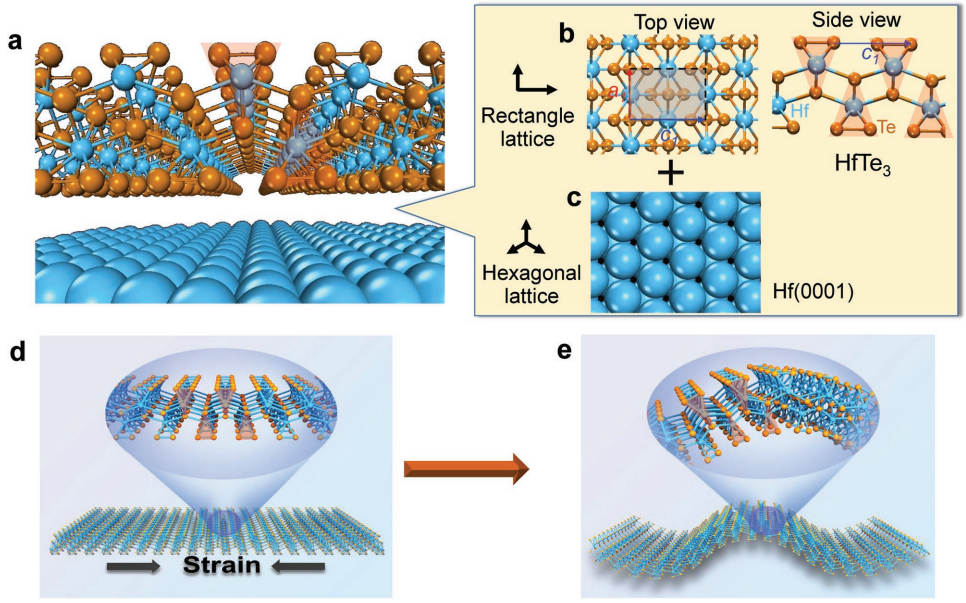

Figure 1. Schematics showing growth process of a wrinkled $HfTe_3$ film. a) Schematic of a flat $HfTe_3$ film on a Hf(0001) substrate. b) The top view (*a*–*c* plane) and side view of a flat $HfTe_3$ film with an anisotropic rectangle lattice. c) The top view of Hf(0001) substrate with isotropic hexagonal lattice. d,e) Schematic diagram of the process from a flat $HfTe_3$ film into a wrinkled film, driven by interfacial strain due to difference in lattices between the $HfTe_3$ film and the substrate.

between the substrate and epitaxial $HfTe_3$ film probably leads to the wrinkles of the film. This symmetric difference brings on the surface strain during the growth of $HfTe_3$ films. Figure 1d,e illustrates the formation of a strain-induced $HfTe_3$ film with a rippled configuration. Our experimental results show the formation of a great many wrinkles in the $HfTe_3$ film grown on Hf(0001) substrate, suggesting that it is an ideal platform to realize the control of topography and related electronic properties in layered 2D materials.

2. Results and Discussion

The growth process of $HfTe_3$ film was first monitored by XPS at different sample temperatures. **Figure 2**a shows the XPS spectra of the Te_{3d} core level before and after sample annealing. In the case that the substrate was kept at room temperature and deposited with Te atoms, the corresponding XPS spectrum shows two peaks (marked by red at binding energies 582.82 and 572.42 eV), indicating no reaction between Te atoms and the substrate. If the substrate was annealed to ≈700 °C, two red peaks disappear and two new peaks appear (marked by the purple at binding energies 583.47 and 573.0 eV). These changes prove the change of the binding energy between elements of Hf and Te, which relates to the reaction between Hf and Te elements. The two purple peaks can be assigned to a $HfTe_3$ film.[21] Moreover, Figure 2b shows the XPS spectra of the Hf_{4f} core level after sample annealing at ≈700 °C. Two peaks (marked by bright blue at binding energies 15.90 and 14.22 eV) in this curve give further evidence of the reaction of as-deposited Te with the Hf substrate, resulting in a $HfTe_3$ film on the substrate, as illustrated by a schematic in Figure 2c. From the XPS spectra of the Hf_{4f} core level in

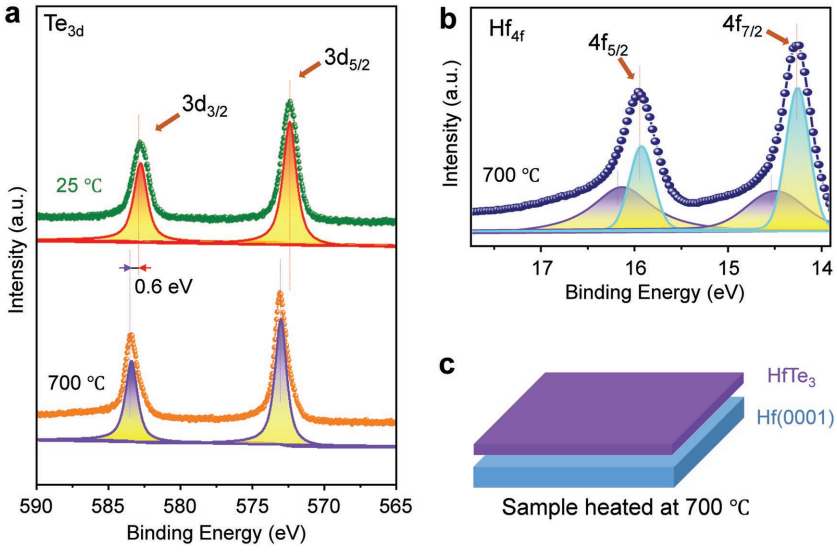

Figure 2. XPS core level measurements before and after sample annealing. a) Red peak at 582.82 and 572.42 eV correspond to the binding energy of Te_{3d} in as-deposited Te clusters on the Hf(0001) substrate at temperature of 25 °C. Purple peaks at 583.47 and 573.0 eV correspond to the binding energy of Te_{3d} in $HfTe_3$ film after sample annealing at 700 °C. b) Purple peaks at 16.23 and 14.56 eV are related to the binding energy of Hf_{4f} in $HfTe_3$ film after sample annealing at 700 °C. Bright-blue peaks at 15.90 and 14.22 eV are related to the binding energy of Hf_{4f} in Hf substrate. c) Schematic drawing of $HfTe_3$ film formed on substrate that was annealed to 700 °C.

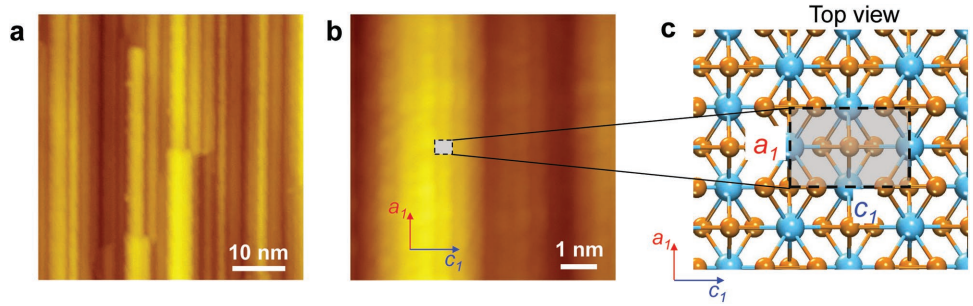

Figure 3. Structural properties of the $HfTe_3$ film. a) STM topographic image (–300 mV, –100 pA) showing plenty of wrinkles in the $HfTe_3$ film. b) High-resolution STM image (–5 mV, –300 pA) of the wrinkles. c) Model from the top view (*a*–*c* plane) of $HfTe_3$ layer with the lattice notation (a_1 and c_1) as that in (b). The dashed rectangle marks a single unit cell of $HfTe_3$ film. One protrusion in the STM image in (b) can be assigned to the topmost Te pairs in the $HfTe_3$ layer.

Figure 2b, we also estimate that the film thickness is less than 2 nm, matching a monolayer of corrugated $HfTe_3$ film on the substrate.

To investigate the atomic structure of the as-grown epitaxial films, the samples were further characterized by STM. **Figure 3**a is a large-scale STM image of $HfTe_3$ film on Hf(0001). There are a great many wrinkles in the film, which originate from the difference of the geometric symmetry between $HfTe_3$ film and the substrate. Figure 3b is a zoom-in image showing details of the wrinkles. The well-ordered protrusions in this image exhibit a rectangular lattice like that of the *a*–*c* plane in $HfTe_3$ bulk (the model is shown in Figure 3c). The periodicity of the STM-observed protrusion in the film is 3.85 Å in the *a*-direction, consistent with the previous experimental report[21] and close to the reported crystal lattice distance of 3.90 Å in $HfTe_3$ bulk.[19,20] Thus, the periodicity of the protrusions almost matches the crystalline lattice in the *a*-direction. With a combination of geometric symmetry and crystalline constant, as well as the experimental evidence from the above XPS data, we conclude that $HfTe_3$ film is formed on the substrate.

In order to analyze the electronic properties of the as-prepared $HfTe_3$ film, we performed STS measurements. The STS method can acquire differential tunneling conductance (dI/dV), which gives a measurement of the local density of states (LDOS) of the $HfTe_3$ film near the Fermi level. **Figure 4**a shows a typical STM image of a $HfTe_3$ wrinkle, and a line profile perpendicular to the wrinkle (marked by a red dashed line) is shown in Figure 4b as well. Five STS curves recorded at different positions along this line are shown in Figure 4c. Curves 1 and 5 are measured at the low-corrugated area. Curves 2–4, which show distinct peaks compared to the curves 1 and 5, are measured at the strained wrinkle. The smaller curvature (like the points 1 and 5) has a weaker LDOS. The larger curvature (like the points 2–4) has a stronger LDOS. There is a positive correlation between the LDOS change and the local wrinkle curvature in this new material. The dI/dV spectrum gives direct access to the local electronic structure of the sample at the position of the STM tip significantly different from the STS measurements at different positions in Figure 4c, demonstrating that the strain-induced wrinkles remarkably affect the electronic structures of the $HfTe_3$ film. Clearly, new electronic states are localized at the wrinkled area.

In order to identify and analyze the observed electronic states, we performed further STS measurements along the direction of a wrinkle (marked by a blue dashed line in Figure 4a). The line profile along the top of this wrinkle is also shown in Figure 4b. Figure 4d shows five STS curves recorded at different positions along this line at the wrinkle. It is very interesting that all these STS curves show similar characteristics in the peak positions and shapes, that is, the local density of states of different positions at the top of the wrinkle show no clear difference. The

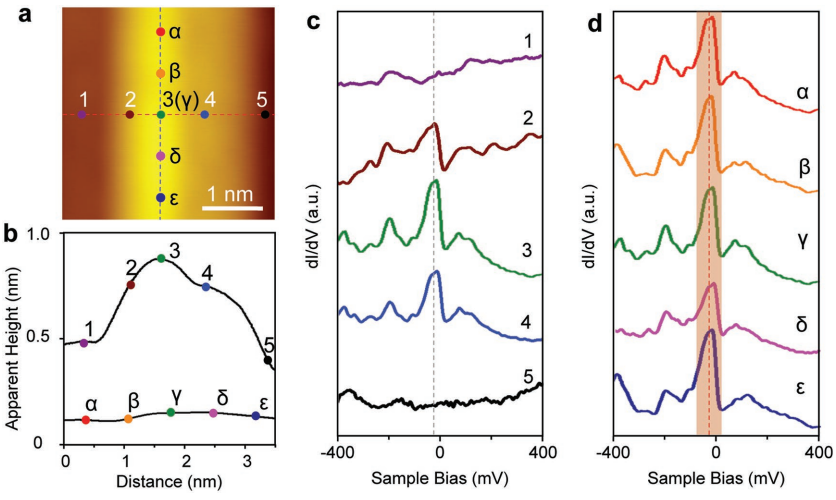

Figure 4. Undulations and electronic properties of the wrinkled $HfTe_3$ film. a) STM topographic image of the $HfTe_3$ wrinkles. b) Line profiles along the dashed lines in (a), illustrating the apparent height of the wrinkles. c) STS measurements obtained at five different positions (marked by Arabic numerals 1, 2, 3, 4, and 5) along the red dashed line in (a). A significant difference exists between STS curve 1 and curves 2–4. Characteristic peaks at the same energies near the Fermi level in curves 2–4 are marked by a black dashed line. d) STS measurements obtained at five different positions (marked by Greek characters α, β, γ, δ, and ε) along the black dashed line in (a), which together show that the curves obtained at different positions have almost the same characteristics. Peaks at the same energies near the Fermi level in the curves are highlighted.

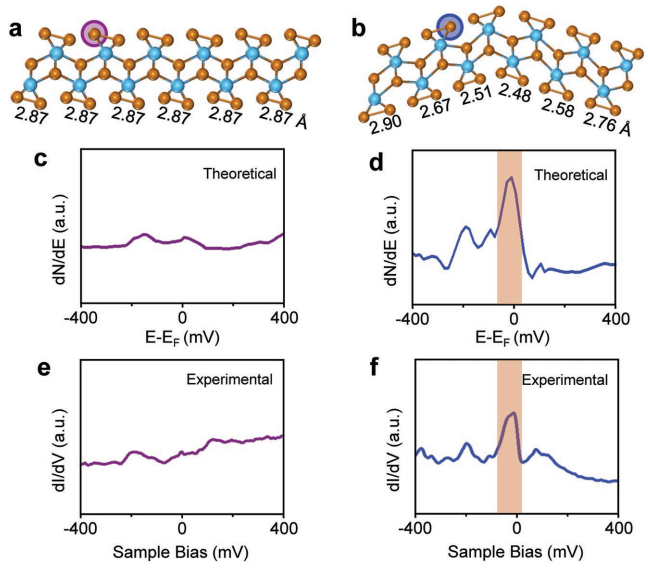

Figure 5. Models of the $HfTe_3$ film, and STS measurements compared to DFT calculations. a,b) Side-view schematics of a flat and a wrinkled $HfTe_3$ layer, respectively. The values of Te–Te bonding lengths, as illustrated, are different in the $HfTe_3$ wrinkle. c,d) Calculated density of states (DOS) at the atoms marked by circles in (a) and (b), respectively. e,f) STS experimental measurements in the flat area and at the wrinkles of the $HfTe_3$ film, respectively.

induced electronic states near the Fermi level exist in the whole wrinkles. Wrinkles form due to the surface strain originating from the symmetry difference of the rectangular $HfTe_3$ film and the hexagonal substrate, which mainly contributes the emergence of characteristic peaks near the Fermi level in STS curves.

To further confirm the causal relationship between the wrinkled configuration and the change of electronic states, we carried out theoretical calculations and simulations. **Figure 5**a,b shows schematic structures of a flat area and a wrinkled area in $HfTe_3$ film, respectively. The binding energy per atom in the wrinkled area is 44 meV lower than that in the strained area, thus the formation of the wrinkles is energetically favorable. The apparent height of the calculated wrinkle in Figure 5b is quite similar to the experimental data, as illustrated by the line profile in Figure 4b. Figure 5c,d shows the calculated local density of states projected from atoms marked by circles in Figure 5a,b, respectively. Figure 5e,f shows STS curves experimentally measured in the flat area and at the wrinkles of the $HfTe_3$ film, respectively. The curve in Figure 5e, measured at a low-corrugated area, is almost the same as the simulated one in Figure 5c, that is, there is no peak near the Fermi level. The measured curve in Figure 5f on the strained wrinkle most resembles the simulated one in Figure 5d, where distinct peaks exist, especially a strong peak at the Fermi level (highlighted by dark yellow). So a combined analysis of STM, STS, and DFT data demonstrates that the surface strain leads to the undulations in $HfTe_3$ film, remarkably, resulting in electronic states in the wrinkles near the Fermi level.

These electronic states are localized in 1D corrugated structures, that is, in the strain-induced wrinkles along a particular direction. One may use these electronic states induced near the Fermi level in practical applications to improve superconductive properties, as previously reported with regard to other materials. ($HfTe_3$ bulk is a superconductor.)[22,23] One also might deposit magnetic atoms on the sample to induce magnetic moments on these wrinkles and use these magnetic-atom-decoration wrinkles as waveguides for spin-waves.[24–26] In addition, the local electrical states would yield heretofore unobserved electrical transport properties, such as different electrical conductivity while the carriers transport across or along these wrinkles. One can develop wrinkle-based heterojunctions that have the same structures and chemical components at the two sides of the junction, quite unlike earlier heterojunctions with different structures or chemical components at the two sides of the junction.[13,27]

3. Conclusion

In summary, we showed for the first time a strained configuration in a 2D TMT film with an anisotropic lattice and related electronic properties. Wrinkles in $HfTe_3$ film were constructed on a Hf(0001) substrate by using the geometric difference between the rectangular lattice in the film and the hexagonal lattice in the substrate. The geometric structures and corresponding electronic properties induced by the difference in lattice symmetry were determined by elaborate experimental observations that were in close agreement with our theoretical calculations. At the wrinkles of $HfTe_3$ film, we observed localized electronic states (clear peaks in STS curves) near the Fermi level, demonstrating that the wrinkled $HfTe_3$ film would be an ideal platform to realize and study artificially adjustable properties in 2D materials. Our work on the generation of strain by designing anisotropic growth models provides a novel way to tune electronic properties of related 2D materials that have great potential for improved superconductive properties, as well as the design of waveguides for spin-wave and related nanoelectronic devices.

4. Experimental Section

Sample Preparation: The $HfTe_3$ films were fabricated in an ultrahigh vacuum system, with a base pressure of 2×10^{-10} mbar, equipped with standard molecular beam epitaxy (MBE) capabilities. The Hf(0001) substrate was prepared by several cycles of Ar^+ ion sputtering, followed by annealing treatment until clean surface terraces were obtained in the STM images. Plenty of Te (Sigma, 99.999%) evaporated from a Knudsen cell was deposited on the clean Hf(0001) surface at room temperature. The sample was subsequently annealed at 700 °C for preparation of the $HfTe_3$ structure. The Te atoms escape easily from the substrate at the reaction temperature (700 °C), therefore, more Te atoms were deposited to supplement the Hf—Te reaction. After growth, the samples were in situ transferred to STM equipment and cooled for imaging of topographies and measurement of the electronic properties.

STM Measurements: To obtain the electronic structures of the films, STM experiments were performed using an ultralow-temperature STM system (Unisoku and RHK) operated at a base temperature of 4.8 K. The differential conductance (dI/dV) was measured using lock-in detection of the tunneling current I by adding a 5 mV modulated bias voltage at 973 Hz to the sample bias voltage V.

DFT Calculations: The first principle calculations were carried out by the VASP (Vienna Ab initio Simulation Package)[28] within the generalized

gradient approximation (GGA) of Perdew, Burke, and Ernzerhof (PBE).[29] The kinetic energy cutoff was set as 450 eV for the calculations. The Monkhorst–Pack k-mesh of $3 \times 16 \times 1$ and $1 \times 16 \times 1$ were used in 2D supercell and 1D nanoribbon calculations, respectively. The binding energy per atom in the wrinkled $HfTe_3$ film is 44 meV lower than that in the strained film.

Supporting Information

Supporting Information is available from the Wiley Online Library or from the author.

Acknowledgements

Y.Q.W. and X.W. contributed equally to this work. The authors acknowledge financial support from the National Basic Research Program of China (No.2013CBA01600) and the National Key Research & Development Projects of China (No. 2016YFA0202300), National Natural Science Foundation of China (Nos. 51572290, 61222112, 51325204, and 11334006), and the Chinese Academy of Sciences (Nos. XDB07030100 and 1731300500015).

Received: August 18, 2016
Revised: October 7, 2016
Published online: November 15, 2016

[1] W. Z. Bao, F. Miao, Z. Chen, H. Zhang, W. Y. Jang, C. Dames, C. N. Lau, *Nat. Nanotechnol.* **2009**, *4*, 562.
[2] F. Guinea, M. I. Katsnelson, A. K. Geim, *Nat. Phys.* **2010**, *6*, 30.
[3] N. Levy, S. A. Burke, K. L. Meaker, M. Panlasigui, A. Zettl, F. Guinea, A. H. C. Neto, M. F. Crommie, *Science* **2010**, *329*, 544.
[4] A. P. A. Raju, A. Lewis, B. Derby, R. J. Young, I. A. Kinloch, R. Zan, K. S. Novoselov, *Adv. Funct. Mater.* **2014**, *24*, 2865.
[5] P. Kang, M. C. Wang, P. M. Knapp, S. Nam, *Adv. Mater.* **2016**, *28*, 4639.
[6] Z. H. Ni, T. Yu, Y. H. Lu, Y. Y. Wang, Y. P. Feng, Z. X. Shen, *ACS Nano* **2008**, *2*, 2301.
[7] C. C. Liu, W. X. Feng, Y. G. Yao, *Phys. Rev. Lett.* **2011**, *107*, 4.
[8] J. E. Lee, G. Ahn, J. Shim, Y. S. Lee, S. Ryu, *Nat. Commun.* **2012**, *3*, 8.
[9] H. Liu, A. T. Neal, Z. Zhu, Z. Luo, X. F. Xu, D. Tomanek, P. D. D. Ye, *ACS Nano* **2014**, *8*, 4033.
[10] X. F. Qian, J. W. Liu, L. Fu, J. Li, *Science* **2014**, *346*, 1344.
[11] H. Li, A. W. Contryman, X. F. Qian, S. M. Ardakani, Y. J. Gong, X. L. Wang, J. M. Weisse, C. H. Lee, J. H. Zhao, P. M. Ajayan, J. Li, H. C. Manoharan, X. L. Zheng, *Nat. Commun.* **2015**, *6*, 6.
[12] W. B. Li, J. Li, *Nat. Commun.* **2016**, *7*, 8.
[13] S. Song, D. H. Keum, S. Cho, D. Perello, Y. Kim, Y. H. Lee, *Nano Lett.* **2016**, *16*, 188.
[14] Y. Pan, H. G. Zhang, D. X. Shi, J. T. Sun, S. X. Du, F. Liu, H. J. Gao, *Adv. Mater.* **2009**, *21*, 2777.
[15] C. R. Dean, A. F. Young, I. Meric, C. Lee, L. Wang, S. Sorgenfrei, K. Watanabe, T. Taniguchi, P. Kim, K. L. Shepard, J. Hone, *Nat. Nanotechnol.* **2010**, *5*, 722.
[16] L. A. Ponomarenko, A. K. Geim, A. A. Zhukov, R. Jalil, S. V. Morozov, K. S. Novoselov, I. V. Grigorieva, E. H. Hill, V. V. Cheianov, V. I. Fal'ko, K. Watanabe, T. Taniguchi, R. V. Gorbachev, *Nat. Phys.* **2011**, *7*, 958.
[17] M. Chhowalla, H. S. Shin, G. Eda, L. J. Li, K. P. Loh, H. Zhang, *Nat. Chem.* **2013**, *5*, 263.
[18] H. L. L. Zhuang, R. G. Hennig, *J. Phys. Chem. C* **2013**, *117*, 20440.
[19] L. Brattas, A. Kjekshus, *Acta Chem. Scand.* **1972**, *26*, 3441.
[20] S. Furuseth, L. Brattas, A. Kjekshus, *Acta Chem. Scand.* **1973**, *27*, 2367.
[21] Y. Q. Wang, X. Wu, Y. L. Wang, Y. Shao, T. Lei, J. O. Wang, S. Y. Zhu, H. Guo, L. X. Zhao, G. F. Chen, S. Nie, H. M. Weng, K. Ibrahim, X. Dai, Z. Fang, H. J. Gao, *Adv. Mater.* **2016**, *28*, 5013.
[22] V. V. Struzhkin, Y. A. Timofeev, R. J. Hemley, H. K. Mao, *Phys. Rev. Lett.* **1997**, *79*, 4262.
[23] C. Si, Z. Liu, W. H. Duan, F. Liu, *Phys. Rev. Lett.* **2013**, *111*, 5.
[24] J. Podbielski, F. Giesen, D. Grundler, *Phys. Rev. Lett.* **2006**, *96*, 4.
[25] H. T. Lu, S. Sota, H. Matsueda, J. Bonca, T. Tohyama, *Phys. Rev. Lett.* **2012**, *109*, 5.
[26] J. M. Law, H. J. Koo, M. H. Whangbo, E. Brucher, V. Pomjakushin, R. K. Kremer, *Phys. Rev. B* **2014**, *89*, 8.
[27] M. Y. Li, Y. M. Shi, C. C. Cheng, L. S. Lu, Y. C. Lin, H. L. Tang, M. L. Tsai, C. W. Chu, K. H. Wei, J. H. He, W. H. Chang, K. Suenaga, L. J. Li, *Science* **2015**, *349*, 524.
[28] G. Kresse, J. Furthmuller, *Phys. Rev. B* **1996**, *54*, 11169.
[29] J. P. Perdew, K. Burke, M. Ernzerhof, *Phys. Rev. Lett.* **1996**, *77*, 3865.

